On the Role of Interpolation in the Normalization of Non-Ideal Visible Wavelength Iris Images

Gil Santos and Hugo Proença
Dept. of Computer Science - IT - Networks and Multimedia Group
Universidade da Beira Interior, Covilhã, Portugal
Email: m1214@ubi.pt, hugomcp@di.ubi.pt

***Abstract*—The growth in practical applications for iris biometrics has been accompanied by relevant developments in the underlying algorithms and techniques. Along with the research focused on near-infrared (NIR) cooperatively captured images, efforts are being made to minimize the trade-off between the quality of the captured data and the recognition accuracy on less constrained environments, where images are obtained at the visible wavelength, at increased distances, over simplified protocols and adverse lightning. This paper addresses the effect of the interpolation method, used in the iris normalization stage, in the overall recognition error rates. This effect is stressed for systems operating under less constrained image acquisition setups and protocols, due to higher variations in the amounts of captured data. Our experiments led us to conclude that the utility of the image interpolating methods is directly corresponding to the levels of noise that images contain.**

I. Introduction

One of the most active research areas in biometry seeks to minimize the constraints associated to the recognition process. The use of the iris as main biometric trait is emerging as one of the most recommended, due to the possibility of contactless data acquisition and to its circular and planar shape that makes easy the detection, segmentation and compensation for off-angle capturing. This area - often called *non-cooperative iris recognition* - receives growing attention from the research community (e.g., [1]–[6], [21]).

Independently of the type of used images (NIR or visible wavelength) and of the constraints associated to the acquisition setup, the large majority of the iris recognition methods perform the normalization of the segmented data into a dimensionless pseudo-polar coordinate system through a process known as the "Daugman rubber sheet" (e.g., [7]–[9]). This transforms the segmented iris data into a rectangular block of fixed size and compensates for varying image capturing distances and pupils' sizes. Due to the different amount of data in the segmented ring and in the normalized block, the use of some interpolation method is unavoidable and constitutes the scope of the work described in this paper. However, the role of the normalization stage is stressed for non-cooperative iris recognition purposes, due to significantly higher variations in the amounts of captured data dictated by the higher range of image capturing distances, different perspectives and heterogeneous lighting conditions that determine the size of the pupil.

In this paper we show how the interpolation method used in the normalization process affects the overall performance of the recognition system. We used our implementation of the Daugman's recognition method [7] and varied the type of interpolation method used in the normalization process, having observed the variations in the recognition error rates over two well known visible wavelength iris image datasets [10], [11].

The remaining of this paper has the following structure: Section II overviews the iris recognition process, namely the less constrained iris acquisition setup and the Daugman's approach. Section III briefly overviews the used variants of image interpolation methods, describes the used datasets and discusses the obtained results. Finally, Section IV states the conclusions.

II. Iris Recognition

The large majority of the published iris recognition methods follow the statistical pattern recognition paradigm, and share the structure given in figure 1 The process starts with the segmentation of the iris ring in the close-up eye image. Further, data is transformed into a double dimensionless polar coordinate system, through the above referred *Daugman's Rubber Sheet* process. Regarding the feature extraction stage, existing approaches can be roughly divided into three variants: phase-based [12], zero-crossing [13] and texture-analysis methods [14]. Dauman [12] used multi-scale quadrature wavelets to extract texture phase-based information and obtain an iris signature with 2048 binary components. Boles and Boashash [13] computed the zero-crossing representation of a 1D wavelet at different resolutions of concentric circles. Wildes [14] proposed the characterization of the iris texture through a Laplacian pyramid with four different levels. Finally, in the feature comparison stage, a numeric dissimilarity value is produced, which determines the subjects' identity. Here, it is usual to apply different distance metrics (Hamming [12],

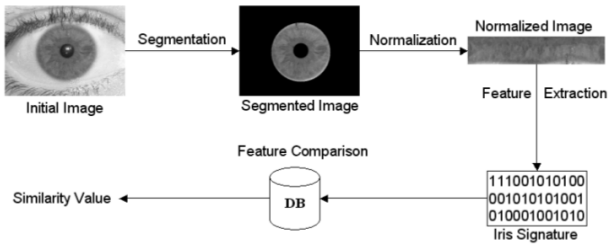

Fig. 1. Typical block diagram of the published iris recognition methods.

Euclidian [15] or weighted Euclidian [16]), or methods based on signal correlation [14].

The accuracy of the deployed iris recognition systems is remarkable, as reported by the study conduced by Daugman [17] and three other independent evaluations [18]–[20]. However, we stress that those error rates are conditioned to the acquisition of good quality images, captured in stop-and-stare interfaces, at close imaging distances. Also, failures on this acquisition setup cause significant increment of the recognition error rates.

A. Less Constrained Image Acquisition

In less constrained conditions, where a trade-off between data acquisition constrains and recognition accuracy is inevitable, the challenge is to maximally increase flexibility in three axes: subjects position and movements, imaging distances and lightning conditions. As before stated, this area receives growing interests from the research community and constituted the scope of several publications. The "Iris-on-the-move" project [2] is a major example of the engineering image acquisition required to make the recognition process less intrusive to subjects. *Honeywell Technologies* registered a patent [3] of a similar system capable of performing at-a-distance iris recognition. Previously, Fancourt et al. [4] showed that it is possible to acquire images at-a-distance of up to 10 meters with sufficient quality to support iris recognition and Narayanswamy and Silveira [5] increased the iris image depth-of-field through a simple framework composed by a camera with fixed focus, without a zoom lenses. Park and Kim [21] proposed an approach to fast at-a-distance acquisition of iris images and He *et al.* [6] studied the acquisition of in-focus images, as well analyzed the impact of different wavelengths in the recognition error rates. Although concluding that illumination inside the 700-900 nm optimally reveals the richness of the iris structure, they observed that irises with moderate levels of pigmentation could be imaged in the visible light with good quality.

B. Daugman's Approach

The Daugman's approach [7] to perform the iris biometric recognition is known to be the most widely acknowledged, with great acceptance over the scientific community. Apart from being the uniquely implemented in commercially deployed systems, it is the one that usually acts as comparison term for alternative proposals.

The structure of this method is as follows: it starts by the detection and segmentation of the iris, through the determination of its circular contours. Later, the normalization of the segmented region is made as described in subsection II-C. The next stage is iris feature extraction through the convolution of the normalized data with a bank of 2D Gabor Wavelets (1), followed by the quantization that gives a binary *iriscode*. This code is used in the matching stage, using the *Hamming Distance* (2) as comparison measure.

$$h_{\{Re,Im\}} = sgn_{\{Re,Im\}} \int_{\rho}\int_{\phi} I(\rho,\phi) e^{iw(\theta_0-\phi)} . \\ .e^{-(r_0-\rho)^2/\alpha^2} e^{-(\theta_0-\phi)^2/\beta^2} \rho d\rho d\phi \tag{1}$$

$$HD = \frac{\|(codeA \otimes codeB) \cap maskA \cap maskB\|}{\|maskA \cap maskB\|} \tag{2}$$

The performance can be accessed by its decidability (3), that reflects the distance between the two distributions obtained for the comparisons between signatures extracted from the same (*intra-class*) and different persons (*inter-class*).

$$d' = \frac{|\mu_{inter} - \mu_{intra}|}{\sqrt{\frac{\sigma^2_{inter} + \sigma^2_{intra}}{2}}} \tag{3}$$

Where μ_{inter} and μ_{intra} denote the means of the inter- and intra-class comparisons and σ_{inter} and σ_{intra} the respective standard deviations.

C. Image Normalization

As mentioned before, the normalization process aims to obtain invariance to size, position and pupil dilatation in the segmented iris region. This is accomplished by assigning each pixel to a pair of real coordinates (r, θ) over the polar coordinates system, which will be used in the later stages.

For this purpose, we will proceed with Daugman's rubber-sheet model [22], as originally proposed. (4) and (5) give a transformation similar to the depicted in figure 1.

$$I(x(r,\theta), y(r,\theta)) \rightarrow I(r,\theta) \tag{4}$$

$$\begin{aligned} x(r,\theta) &= (1-r)x_p(\theta) + r x_s(\theta) \\ y(r,\theta) &= (1-r)y_p(\theta) + r y_s(\theta) \end{aligned} \tag{5}$$

Where r and θ denote respectively the radius and the angle, $x(r,\theta)$ and $y(r,\theta)$ are defined as linear combinations of both the set of pupillary boundary points $(x_p(\theta), y_p(\theta))$ and the set of limbus boundary points along the outer perimeter of the iris $(x_s(\theta), y_s(\theta))$ bordering the sclera.

III. Experiments

The use of the Daugman's recognition method should be justified. Although this method has been thought to operate over iris images acquired at NIR wavelengths, it has proven to perform well in different types of images, specially if the iris was accurately segmented and occlusions of the iris textures are detected and localized in the original and normalized data. The necessary parameters for the Gabor wavelets (1) were tuned for best performance on all different trials, being chosen those with maximal decidability (3). Regarding iris' location and segmentation, all images were manually and accurately segmented, being known the center and radius of the pupils and of the iris and detected the regions that occlude portions of the iris. Thus, we assume that segmentation inaccuracies and noisy regions do not corrupt the obtained results.

A. Image Interpolation Methods

On the translation between the cartesian and the pseudo-polar coordinate system we used three interpolation variants. The first - hereinafter called *no interpolation* - simply picks from the cartesian data the nearest neighbor pixel of $(x(r,\ \theta), y(r,\ \theta))$ (using L_2 norm). Also, we implemented two of the most well known interpolation variants: the bilinear and bicubic [23], which obtain the corresponding value according to its neighborhood, as below described. Other types of interpolation (as the bicubic splines) were not the focus of our analyzis, essentially because we believe that the obtained results will be close to those obtained.

1) Bilinear Interpolation: This is the simplest method to perform the two-dimensional approximation of missing values.

$$y(x_1, x_2) = (1-t)(1-u)y_0 + t(1-u)y_1 + tuy_2 + (1-t)uy_3 \tag{6}$$

To determine the value $y_{ij} = y(x_{1i}, x_{2j})$ at some point, (6) is used, considering four surrounding points $y_o, ..., y_3$, defined counterclockwise starting from the lower left that obey the relations stated in (7) with i and j according to (8) and t, u as described in (9).

$$\begin{aligned} y_0 &\equiv y_{ij} & y_1 &\equiv y_{(i+1)j} \\ y_2 &\equiv y_{(i+1)(j+1)} & y_3 &\equiv y_{i(j+1)} \end{aligned} \tag{7}$$

$$x_{1i} \leq x_1 \leq x_{1(i+1)} \qquad x_{2j} \leq x_2 \leq x_{2(j+1)} \tag{8}$$

$$\begin{aligned} t &\equiv (x_1 - x_{1i})/(x_{1(i+1)} - x_{1i}) \\ u &\equiv (x_2 - x_{2j})/(x_{2(j+1)} - x_{2j}) \end{aligned} \tag{9}$$

2) Bicubic Interpolation: This interpolation method gives an higher order of smoothness, at a cost of use a higher number of pixels in each operation. Interpolation for the function y, given the four derivatives y_1, y_2, y_{12}, is executed in two steps: determination of quantities $c_{ij}, i, j = 0, ..., 3$ combining a region of the image with the appropriate matrix, and then the following equations (10) with t, u given by (9).

$$\begin{aligned} y(x_1, x_2) &= \sum_{i=0}^{3}\sum_{j=0}^{3} c_{ij} t^i u^j \\ y_1(x_1, x_2) &= \sum_{i=0}^{3}\sum_{j=0}^{3} i c_{ij} t^{i-1} u^j (dt/dx_1) \\ y_2(x_1, x_2) &= \sum_{i=0}^{3}\sum_{j=0}^{3} j c_{ij} t^i u^{j-1} (du/dx_2) \\ y_{12}(x_1, x_2) &= \sum_{i=0}^{3}\sum_{j=0}^{3} ij^3 c_{ij} t^{i-1} u^{j-1} \end{aligned} \tag{10}$$

B. Datasets

In the experiments, two different datasets were used: Ubiris and Ubiris.v2. The higher range of image acquisition distances enables the capturing of irises with higher varying sizes and will make the results more visible. Also, our research concerns the feasibility of recognition in visible wavelength iris images, captured at-a-distance and on-the-move.

The Ubiris database [10] was created at the Soft Computing and Image Analysis Lab (*SOCIA Lab*) of the University of Beira Interior. It consists on a set of visible wavelength noisy iris images, captured at close-up distance with user cooperation. This dataset is intended for the development of robust iris recognition algorithms for biometric purposes and aims to *simulate* non-cooperative image acquisition, adding noise to the resultant images.

The Ubiris.v2 [11], also created at *SOCIA Lab*, contains images *actually* captured at-a-distance (between 4 and 8 meters) from moving subjects. Those images contain several regions of the iris rings occluded by reflections, as well significant iris obstructions due to eyelids and eyelashes.

Over 500 pictures (400×300 pixels) were used from each dataset on our experiments. In both cases, we selected a group of images that we believe to represent each dataset.

C. Results and Discussion

1) Cartesian Data Usage: Our first observation is that the interpolating methods used in the normalization process do impact over iris pixels usage. To illustrate this, figure 2 shows the number of times each pixel located within the ring of a segmented iris region is used in the translation into the normalized data. Here, brighter pixels denote those more frequently accessed. The higher smoothness of the image corresponding to the bicubic interpolation is evident, as well evident discontinuities in the pixels' usage can be observed in the left image, obtained when used the no interpolation variant.

Not surprisingly, we observed that the average probability of a pixel to be used in the normalization process remains stable (due to the fixed size of the normalized block). However, the standard deviation obtained for the corresponding distribution becomes significantly lower when interpolation methods are used. In other words, pixel selection during a normalization process became more balanced, directly corresponding to the complexity of the interpolation process, i.e., to the number of pixels involved in a single interpolating operation.

Figures 3 and 4 give histograms about the probability for the pixels usage in the normalization stages, respectively in the Ubiris and Ubiris.v2 data sets. The horizontal axis gives the probability beans and the vertical gives the number of pixels that fall in the corresponding bean.

Regarding the Ubiris dataset (highly normalized), it can be observed a considerable reduction in the amount of pixels that were never accessed during the normalization procedure (#pix-

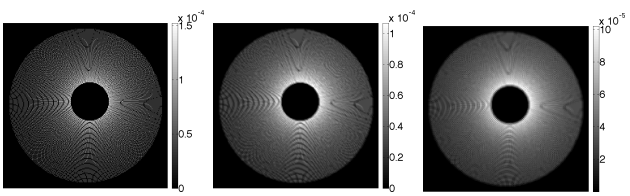

Fig. 2. Representation of the number of times that each pixel of the segmented iris data is accessed during a normalization process, when using no interpolation (left), the bilinear (middle) and the bicubic (right) interpolation.

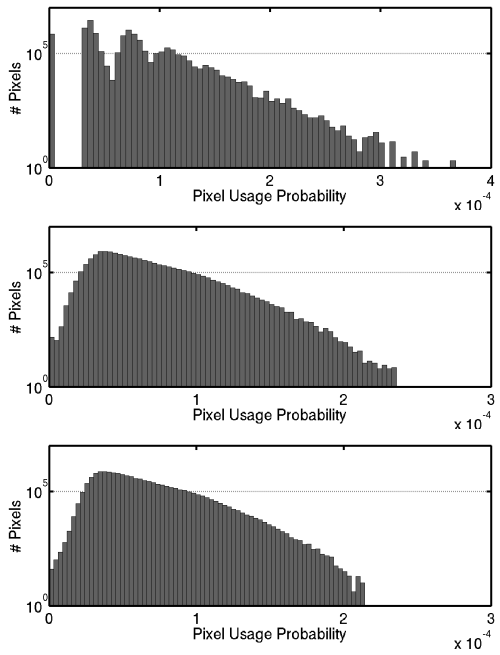

Fig. 3. Overall probability for the iris pixel usage respectively with no interpolation (top), bilinear (middle) and bicubic interpolation (bottom) in the Ubiris dataset.

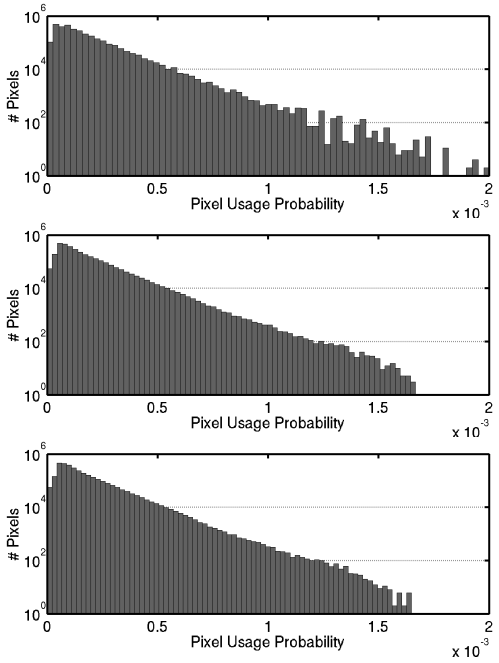

Fig. 4. Overall probability for the iris pixel usage respectively with no interpolation (top), bilinear (middle) and bicubic interpolation (bottom) in the Ubiris.v2 dataset.

els within the 0 probability bean), as well as an accentuation of the slope of the #Pixels value regarding the augment of the probability values.

The spread of the bar beans also suffers an decrement, from the no-interpolation to the bilinear and from this one to the bicubic variant. Using the bilinear interpolation, the probability for the pixel selection converged to a more evenly distributed iris data usage, where pixels are more likely to became part of the data used to extract the iriscode. Finally, when analyzing the bicubic interpolation, these changes are even more visible. The amplitude of the overall distribution was smaller and more homogeneous, as well as the resemblance between the probability for the pixel selection and a normal distribution.

Interestingly, the values obtained for the Ubiris.v2 database were more close to each other, which we explain by the higher irregularity of this data set. However, the above stated observations for the first version of the database fit to the results obtained for this second version, as can be seen essentially by the higher spread of the histogram's beans when no interpolation method was used.

2) Recognition Error Rates: Here, we give results about the variations of the recognition error rates, as function of the type of interpolating method used in the normalization process. We plot the receiver operating curves (ROC) obtained when using each of the three interpolating variants on the two experimented datasets. The first interesting observation is that the lowest error rates in the Ubiris data set were - clearly - obtained when no interpolation method was used (figure 5). Our interpretation is that less cartesian iris pixels are used in the normalized data, which minimizes the aliasing effects induced by the normalization process. Thus, in environments that propitiate the acquisition of less noisy images, the use of interpolating methods represents no-advantage, as showed by the difference between the results obtained when using no-interpolation and the interpolating methods.

Oppositely, for the Ubiris.v2 images the better results were obtained when using the two types of interpolating techniques (figure 6). As this dataset contains higher levels of noise, the normalization process tend to be best succeed if more iris pixels are used in each normalization step, smoothing the corruption that non-detected noisy data carries to the normalized image.

Finally, the previously described usage of the iris pixels of the cartesian coordinate system as function of the interpolation method is resumed in Table I, with corresponding confidence

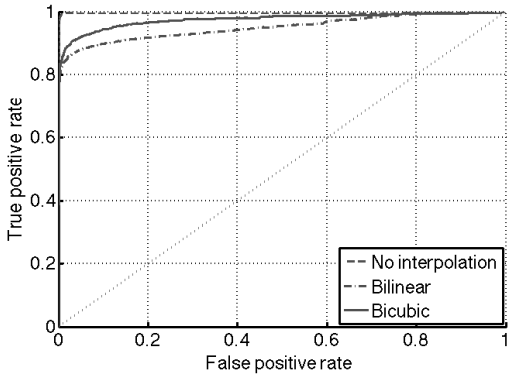

Fig. 5. ROC curve for different interpolation methods on Ubiris dataset.

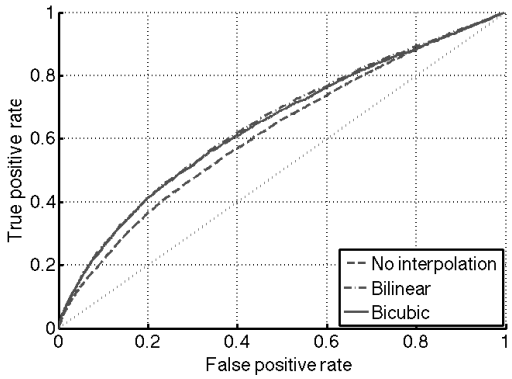

Fig. 6. ROC curve for different interpolation methods on Ubiris.v2 dataset.

intervals of 95%. Also, it is given the decidability (3) of the corresponding pattern recognition systems. That - again - confirms the previously stated conclusions: the use of image interpolation techniques on less noisy images seems not to represent any surplus in the final error rates. However, if images are highly noisy, interpolation techniques can slightly increase the recognition accuracy.

	Interpolation	Iris Usage	Decidability
Ubiris	None	$0.926 \pm 1.663 \times 10^{-4}$	4.390
	Bilinear	$0.999 \pm 2.294 \times 10^{-6}$	2.724
	Bicubic	$0.999 \pm 6.362 \times 10^{-7}$	2.779
Ubiris.v2	None	$0.967 \pm 1.957 \times 10^{-4}$	0.410
	Bilinear	$0.986 \pm 1.286 \times 10^{-4}$	0.519
	Bicubic	$0.988 \pm 1.209 \times 10^{-4}$	0.496

TABLE I
IRIS PIXEL USAGE AND DECIDABILITY ON DIFFERENT INTERPOLATION METHODS FOR UBIRIS AND UBIRIS.V2 DATASET.

IV. CONCLUSIONS

Although usually not mentioned, the interpolation technique used in the translation of the segmented iris data between coordinate systems can impact the final error rates of the recognition system. In this paper we used the Daugman's recognition method and two data sets with different levels of noise to evaluate the variations in the recognition error rates, as function of three image interpolating variants: nearest neighbor (no-interpolation), bilinear and bicubic.

We concluded that the use of interpolation techniques does not constitute any significant advantage in iris images with low levels of noise and tend to contribute to a slightly decrease in the recognition error rates of highly noisy iris images. Thus, further research is required to access the utility of these interpolating techniques in the increase of the recognition robustness, on non-cooperative iris recognition environments, where the ability to deal with highly noisy and heterogeneous iris data is required.

ACKNOWLEDGMENT

We acknowledge the financial support given by "FCT-Fundação para a Ciência e Tecnologia" and "FEDER" in the scope of the PTDC/EIA/69106/2006 research project "BIOREC: Non-Cooperative Biometric Recognition".

REFERENCES

[1] H. Proença, "On the feasibility on the visible wavelength, at-a-distance and on-the-move iris recognition," *IEEE IEEE Symposium Series on Computational Intelligence in Biometrics: Theory, Algorithms, and Applications*, 2009.

[2] J. R. Matley, D. Ackerman, J. Bergen, and M. Tinker, "Iris recognition in less constrained environments," *Springer Advances in Biometrics: Sensors, Algorithms and Systems*, pp. 107–131, October 2007.

[3] "A distance iris recognition," Honeywell International Inc., Tech. Rep., 2007, united States Patent 20070036397.

[4] C. Fancourt, L. Bogoni, K. Hanna, Y. Guo, R. Wildes, N. Takahashi, and U. Jain, "Iris recognition at a distance," in *Proceedings of the 2005 IAPR Conference on Audio and Video Based Biometric Person Authentication*, U.S.A., July 2005, pp. 1–13.

[5] R. Narayanswamy, G. Johnson, P. Silveira, and H. Watch, "Extending the imaging volume for biometric iris recognition," *Applied Optics*, vol. 44, no. 5, pp. 701–712, February 2005.

[6] Y. He, J. Cui, T. Tan, and Y. Wang, "Key techniques and methods for imaging iris in focus," in *Proceedings of the IEEE International Conference on Pattern Recognition*, August 2006, pp. 557–561.

[7] J. G. Daugman, "How iris recognition works," *IEEE Transactions on Circuits and Systems for Video Technology*, vol. 14, no. 1, pp. 21–30, January 2004.

[8] L. Ma, T. Tan, Y. Wang, and D. Zhang, "Personal identification based on iris texture analysis," *IEEE Transactions on Pattern Analysis and Machine Intelligence*, vol. 25, no. 12, pp. 2519–2533, December 2003.

[9] C. Tisse, L. Martin, L. Torres, and M. Robert, "Person identification technique using human iris recognition," in *Proceedings of the 25th International Conference on Vision Interface*, Calgary, July 2002, pp. 294–299.

[10] H. Proença and L. Alexandre, "Ubiris: A noisy iris image database." in *Proceedings of ICIAP 2005 - Interacional Conference on Image Analysis and Processing, Vol. 1*, 2005, pp. 970–977.

[11] H. Proença, S. Filipe, R. Santos, J. Oliveira, and L. A. Alexandre, "The ubiris.v2: A database of visible wavelength iris images captured on-the-move and at-a-distance," *IEEE Transactions on Pattern Analysis and Machine Intelligence*.

[12] J. G. Daugman, "Phenotypic versus genotypic approaches to face recognition," in *Face Recognition: From Theory to Applications*. Heidelberg: Springer-Verlag, 1998, pp. 108–123.

[13] W. W. Boles and B. Boashash, "A human identification technique using images on the iris and wavelet transform," *IEEE Transactions on Signal Processing*, vol. 46, no. 4, pp. 1185–1188, April 1998.

[14] R. P. Wildes, "Iris recognition: an emerging biometric technology, vol. 85, no. 9," in *Proceedings of the IEEE*, U.S.A., September 1997, pp. 1348–1363.

[15] Y. Huang, S. Luo, and E. Chen, "An efficient iris recognition system," in *Proceedings of the First International Conference on Machine Learning and Cybernetics*, China, November 2002, pp. 450–454.

[16] L. Ma, T. Tan, Y. Wang, and D. Zhang, "Local intensity variations analysis for iris recognition," *Pattern recognition, vol. 37, no. 6*, pp. 1287–1298, 2004.

[17] J. G. Daugman, "New methods in iris recognition," *IEEE Transactions on Systems, Man, and Cybernetics - Part B: Cybernetics*, vol. 37, no. 5, pp. 1167–1175, 2007.

[18] J. L. Cambier, "Iridian large database performance," Iridian Technologies, Tech. Rep., 2007, http://iridiantech.com.

[19] "Independent test of iris recognition technology," International Biometric Group, Tech. Rep., 2005, http://www.biometricgroup.com.

[20] T. Mansfiel, G. Kelly, D. Chandler, and J.Kane, "Biometric product testing and final report, issue 1.0," 2001.

[21] K. Park and J. Kim, "A real-time focusing algorithm for iris recognition camera," *IEEE Transactions on Systems, Man and Cybernetics*, vol. 35, no. 3, pp. 441–444, August 2005.

[22] J. G. Daugman, "High confidence visual recognition of persons by a test of statistical independence," *IEEE Transactions on Pattern Analysis and Machine Intelligence*, vol. 25, no. 11, pp. 1148–1161, November 1993.

[23] W. H. Press, S. A. Teukolsky, W. T. Vetterling, and B. P. Flannery, *Numerical Recipes 3rd Edition: The Art of Scientific Computing*. U.K.: Cambridge University Press, 2007.